Elastic constants and anisotropy in FeNi alloys at high pressures from first-principles calculations

C. Asker*
Department of Physics, Chemistry and Biology (IFM), Linköping University, SE-581 83 Linköping, Sweden

L. Vitos
Department of Materials Science and Engineering, Applied Materials Physics, The Royal Institute of Technology, SE-10044 Stockholm, Sweden;
Department of Physics and Materials Science, Division for Materials Theory, Uppsala University, P.O. Box 530, SE-751 21 Uppsala, Sweden;
and Research Institute for Solid State Physics and Optics, P.O. Box 49, H-1525 Budapest, Hungary

I. A. Abrikosov
Department of Physics, Chemistry and Biology (IFM), Linköping University, SE-581 83 Linköping, Sweden
(Received 25 March 2009; revised manuscript received 29 May 2009; published 19 June 2009)

The single-crystal and polycrystalline elastic constants and the elastic anisotropy in face-centered cubic and hexagonal close-packed FeNi alloys have been investigated at ultrahigh pressures by means of first-principles calculations using the exact muffin-tin orbitals method and the coherent-potential approximation. Comparisons with earlier calculations for pure Fe and experimental results are presented and discussed. We show that Ni alloying into Fe increases slightly the density and has very little effect on bulk moduli. Moreover, the relative decrease in c_{44} elastic constant is much stronger in the hcp phase than in the fcc one. It is found that the elastic anisotropy is higher for face-centered cubic than for the hexagonal close-packed structure of FeNi, even though the face-centered cubic phase has a higher degree of symmetry. The anisotropy in face-centered cubic structure decreases with increasing nickel concentration while a very weak increase is observed for the hexagonal close-packed structure.

DOI: 10.1103/PhysRevB.79.214112 PACS number(s): 62.20.de, 62.20.dq, 62.50.−p

I. INTRODUCTION

The influence of pressure on materials properties is an important field of condensed-matter physics, which currently attracts much attention. In particular, the elastic properties of materials at high pressure change substantially and knowledge of their behavior provide information on the stability of a system, on the propagation of sound waves, and on the elastic anisotropy. But the available information on materials properties at such ultrahigh-pressure conditions is limited. Indeed, the pressure that currently can be reached experimentally in studies of, for instance, FeNi alloys using the diamond-anvil cells is on the order of 250 GPa.[1] At higher compressions the lack of experimental data should be compensated by theoretical simulations based on accurate first-principles theories. Note that iron and iron-based alloys are thought to be the main constituents of the earth's core. Therefore a study of such systems at conditions resembling those of the core is of great importance for several branches of science, including physics, geophysics, and geochemistry.

In recent years there have been numerous works published on the lattice stability of pure Fe and Fe-based alloys at ultrahigh-pressure conditions[1–9] which have discussed the possible structure and composition of the core. Moreover, the elastic properties of Fe and ordered Fe-based compounds at the earth's core conditions have been investigated theoretically in several recent publications.[4,7,10–12] While important, we feel that there is a need to include more complex systems, e.g., disordered Fe-based alloys since this is likely to influence the picture.[13]

In this work we present first-principles theoretical results for the elastic properties of Fe and FeNi systems at high pressures. The calculations have been done at zero temperature, neglecting the effect of lattice vibrations. We employ the exact muffin-tin orbitals Method (EMTO) with the coherent-potential approximation (CPA), that has been proven to be a reliable tool for the calculation of the elastic properties of alloys, predicting their values with accuracy within 10%,[14–16] which is typical for state-of-the-art first-principles calculations[17] and giving very accurate description of the concentration dependencies. There has been many different studies of Fe and Ni using the CPA method[18–26] and the method is therefore known to be reliable for our setup. We emphasize the accurate description of disorder effects and view this study as the first step toward the development of a reliable model that includes the effects of disorder, compression, and high temperature at the same footing. We have studied the elastic properties of fcc and hcp FeNi alloys since they both are suggested as possible candidates for the earth's core structure.[6,8] Though, while at high pressure and high temperatures the bcc structure of Fe is competitive to the fcc and hcp, it is dynamically unstable at low temperatures and high pressures[1,2,4,9] and therefore is not included in this study. From the single-crystal elastic constants, we compute the polycrystalline elastic moduli and the anisotropy as function of pressure and Ni concentration.

The paper is organized in the following way: in Sec. II we briefly present the theory used for the calculation of elastic properties of FeNi alloys and later in Sec. III we outline the method used for the first-principles calculations along with practical details of the calculations. In Secs. IV A–IV C the results for the equation of state (EOS), the single-crystal

elastic properties, and anisotropy is presented, respectively. We summarize the results in Sec. V.

II. THEORY

A. Equation of state

For both fcc and hcp phases, the first step in calculating the elastic properties has been to find the EOS. In the case of fcc alloys, it can be done by calculating the total energy for a set of volumes. From this the ground-state volume can readily be found and also the pressure (P) and bulk modulus (B) as functions of the volume (V). In hcp alloys, the c/a ratio must first be determined for each volume, V by minimizing the energy $E(V,c/a)$ versus c/a, and then the EOS is computed using the energy minima $E(V,c/a)$.

In this work the third order Birch-Murnaghan EOS (Ref. 27) has been used for fitting the theoretical data since it is most often used in experimental studies of solids at high pressure.

B. Elastic constants

The elastic constants have been calculated using *volume-conserving* distortions. Using volume-conserving deformations allows us to identify the calculated elastic constants with the stress-strain coefficients used for wave-propagation velocity.[28–30] Also, it is important for maintaining high accuracy in the calculations since the total energy depends stronger on volume than on the distortions.[28]

1. Face-centered cubic alloys

For the fcc structure, there are three independent elastic constants: c_{11}, c_{12}, and c_{44}.[31] Two of these can be derived from the bulk modulus

$$B = \frac{c_{11} + 2c_{12}}{3}, \tag{1}$$

and the so-called Zener's elastic constant c',

$$c' = \frac{c_{11} - c_{12}}{2}. \tag{2}$$

The c_{11} and c_{12} elastic constants are derived from Eqs. (1) and (2). The c' elastic constant was obtained using the orthorhombic deformation,[16]

$$\mathbf{I} + \mathbf{D_O} = \begin{pmatrix} 1+\delta & 0 & 0 \\ 0 & 1-\delta & 0 \\ 0 & 0 & \frac{1}{1-\delta^2} \end{pmatrix} \tag{3}$$

yielding the following change in the total energy:

$$\Delta E/V = 2c' \cdot \delta^2 + \mathcal{O}(\delta^4). \tag{4}$$

The c_{44} elastic constant can be calculated from the monoclinic distortion,[16]

$$\mathbf{I} + \mathbf{D_M} = \begin{pmatrix} 1 & \delta & 0 \\ \delta & 1 & 0 \\ 0 & 0 & \frac{1}{1-\delta^2} \end{pmatrix} \tag{5}$$

corresponding to the energy change in

$$\Delta E/V = 2c_{44} \cdot \delta^2 + \mathcal{O}(\delta^4). \tag{6}$$

2. Hexagonal close-packed alloys

In hcp crystals there are five independent elastic constants, c_{11}, c_{12}, c_{13}, c_{33}, and c_{44}. From the calculation of the EOS (see above), the c/a ratio as function of volume is known as $[(c/a)=(c/a)(V)]$ and also the bulk modulus can be evaluated. From $E(V,c/a)$ two auxiliary elastic constants, c_S and R can be obtained as

$$c_s = \frac{9(c/a)^2}{V} \left. \frac{\partial^2 E(V,c/a)}{\partial (c/a)^2} \right|_{c/a=(c/a)(V)}, \tag{7}$$

$$R = -\frac{d \ln (c/a)(V)}{d \ln V}. \tag{8}$$

The c_{44} elastic constant can be obtained from the volume-conserving monoclinic distortion,

$$\mathbf{I} + \mathbf{D_M} = \begin{pmatrix} 1 & 0 & \delta \\ 0 & \frac{1}{1-\delta^2} & 0 \\ \delta & 0 & 1 \end{pmatrix} \tag{9}$$

and the corresponding change in energy is

$$\Delta E/V = 2c_{44} \cdot \delta^2 + \mathcal{O}(\delta^4). \tag{10}$$

$c_{66}=(c_{11}-c_{12})/2$ can be obtained from the following volume-conserving distortion:

$$\mathbf{I} + \mathbf{D_O} = \begin{pmatrix} 1+\delta & 0 & 0 \\ 0 & 1-\delta & 0 \\ 0 & 0 & \frac{1}{1-\delta^2} \end{pmatrix} \tag{11}$$

and the energy change is

$$\Delta E/V = 2c_{66} \cdot \delta^2 + \mathcal{O}(\delta^4). \tag{12}$$

Now, since

$$c_s = c_{11} + c_{12} + 2c_{33} - 4c_{13},$$

$$R = \frac{c_{33} - c_{11} - c_{12} + c_{13}}{c_s}, \tag{13}$$

all elastic constants for an hcp crystal can be obtained from c_{44}, c_{66}, c_s, R, and B_{mod} using the above relations.[16]

3. Polycrystalline elastic constants and elastic anisotropy

For the fcc structure, the Voigt and Reuss bulk moduli are equivalent with the single-crystal bulk modulus from Eq. (1). The Voigt and Reuss shear moduli are given by[31]

$$G_V = \frac{c_{11} - c_{12} + 3c_{44}}{5} = \frac{2c' + 3c_{44}}{5}, \tag{14}$$

$$G_R = \frac{5(c_{11} - c_{12}) \cdot c_{44}}{4c_{44} + 3(c_{11} - c_{12})} = \frac{5c' c_{44}}{2c_{44} + 3c'}. \tag{15}$$

For the hcp structure, the Voigt and Reuss bulk moduli are different (how much depends on how strongly c/a depends on volume) and defined as

$$B_V = \frac{2(c_{11}+c_{12})+4c_{13}+c_{33}}{9}, \tag{16}$$

$$B_R = \frac{c^2}{c_s}, \tag{17}$$

where $c^2 = c_{33}(c_{11}+c_{12}) - 2c_{13}^2$. B_R is obtained from the EOS calculations.

For the hcp crystal, the Voigt and Reuss shear moduli are defined as follows:[31]

$$G_V = \frac{12c_{44}+12c_{66}+c_s}{30}, \tag{18}$$

$$G_R = \frac{5}{2}\frac{c_{44}c_{66}c^2}{(c_{44}+c_{66})c^2 + 3B_V c_{44}c_{66}}. \tag{19}$$

The Voigt and Reuss shear moduli can be used to calculate the *Voigt-Reuss-Hill* (VRH) anisotropy, defined as[31]

$$A_{\mathrm{VRH}} = \frac{G_V - G_R}{G_V + G_R}. \tag{20}$$

With this definition A_{VRH} is zero for isotropic crystals and its deviation from zero gives a measure of the anisotropy.[16] We would like to point out that unlike the single-crystal anisotropy ratios (e.g., the Zener of every ratios) The VRH anisotropy ratio is suitable to compare the anisotropies of different crystal structures.

III. DETAILS OF THE CALCULATIONS

A. Electronic structure calculations

The present calculations are based on *density-functional theory*,[32,33] in combination with the *local-density approximation* (LDA) as parametrized by Perdew, Burke, and Ernzerhof.[34] The total energy is calculated using the *full-charge-density technique*.[16,35] In addition to the LDA, the total energy is calculated within the *generalized gradient approximation* (GGA) (Ref. 34) using the electron density obtained from the LDA self-consistent calculation. For nonmagnetic systems this procedure provides essentially the same materials properties as those of a self-consistent GGA scheme.

Furthermore, the electronic structure problem is solved using the EMTO.[36–38] The treatment of a random substitutional alloy is done through the CPA.[39,40] The EMTO-CPA (Ref. 14) method has proven to be accurate enough for calculation of elastict properties of alloys[13,14] while demanding reasonable computational resources.

B. Computational setup

Since this work deals with FeNi at high pressure, the calculations were all nonmagnetic. From a study of magnetism in FeNi alloys[26] we know that at pressures above about 50 GPa fcc FeNi is nonmagnetic, at least in the concentration range presented in this paper. Also, calculations by Steinle-Neumann *et al.*[41] show that hcp Fe is nonmagnetic above about 75–80 GPa.

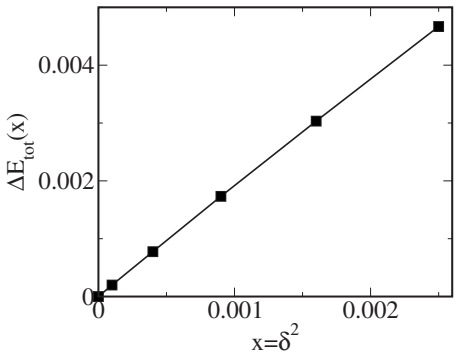

FIG. 1. Example of the difference in total energy as function of the square of the lattice distortion.

The EMTO calculations were performed using 16 complex energy points for the Green's function integration and the basis set contained s, p, d, and f orbitals. The k-space sampling of the irreducible part of the Brillouin zone was done by $25\times25\times25$ points for the fcc crystals and by $17\times17\times13$ (EOS and c_{66}) and $16\times16\times10$ (c_{44}) points for hcp, respectively. These figures roughly correspond to the same density of points in k space for all structures. The k-point convergence was verified against the elastic constants since they are numerically more sensitive compared to the total energies and the EOS.

For the EOS part, the total energy was calculated for the Wigner-Seitz radii $R_{\mathrm{ws}}=\{2.10,2.15,\ldots,2.55,2.60\}$ Bohr corresponding to the atomic volumes $V\approx\{38.8,41.6,44.6,47.7,51.0,54.4,57.9,61.6,65.4,69.5,73.6\}$ Bohr^3. The energy-volume curve was then fitted to a Birch-Murnaghan[27] EOS, as mentioned above. For consistency, this equation of state was also checked against the modified Morse[42] EOS. The above Wigner-Seitz radii were also used for the calculation of elastic constants.

When calculating the elastic constants, the distortions in Eqs. (3), (5), (9), and (11) were $\delta=\{0.00,0.01,\ldots,0.05\}$. Then the elastic constants were obtained by linear fit of the energy as function of the square of the distortions (δ^2), Eqs. (4), (6), (10), and (12). Figure 1 shows an example which illustrates this procedure. Fitting of the square of the distortion is more stable numerically than fitting the distortion.

IV. RESULTS

A. Equation of state

Figure 2 shows the calculated EOS for fcc $Fe_{80}Ni_{20}$ alloy and pure Fe. The lack of experimental data for the fcc phase at high pressure does not allow us to make any comparison with experiment. At a fixed volume (about $\sim$51 Bohr^3 per atom) the pressure increases when going from pure Fe to the $Fe_{75}Ni_{25}$ alloy. Similar behavior is observed for the other volume points in the high-pressure region, though the difference is volume dependent.

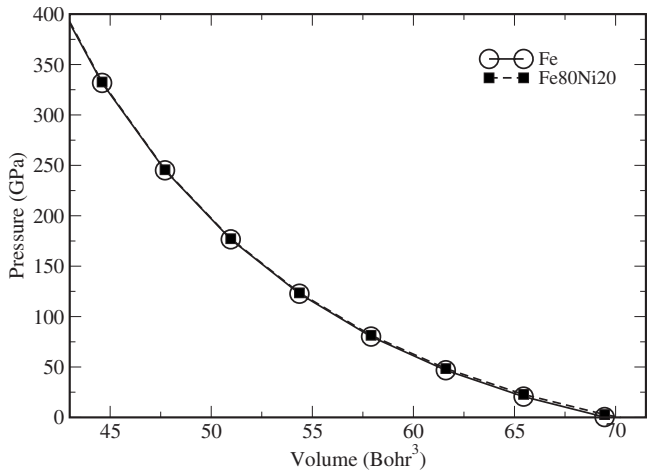

FIG. 2. Pressure as function of volume in fcc $Fe_{80}Ni_{20}$ (dashed lines) and pure Fe (full lines).

Figure 3 shows the EOS for hcp $Fe_{80}Ni_{20}$ alloy and pure Fe. Also, results from other theoretical works are shown (Ref. 41) together with experimental results (Refs. 43–45). The agreement with calculations of Ref. 41 is very good, which is expected since both calculations are nonmagnetic. Below about 75–80 GPa magnetism and/or correlation effects may influence the equation of state,[26,41] which can be seen from the increasing deviation between the calculations and the experiment data. But at higher pressure the agreement with experiment is very good and this is the pressure region of interest for this work. The change in the EOS with changing Ni concentration is rather small. This is expected since Fe and Ni have a small size mismatch and also quite similar electronic structure. The pressure for a certain volume (~51 Bohr^3) increases only about 1.5% when going from pure Fe to $Fe_{75}Ni_{25}$. Similar behavior is observed for the other volume points in the high-pressure region.

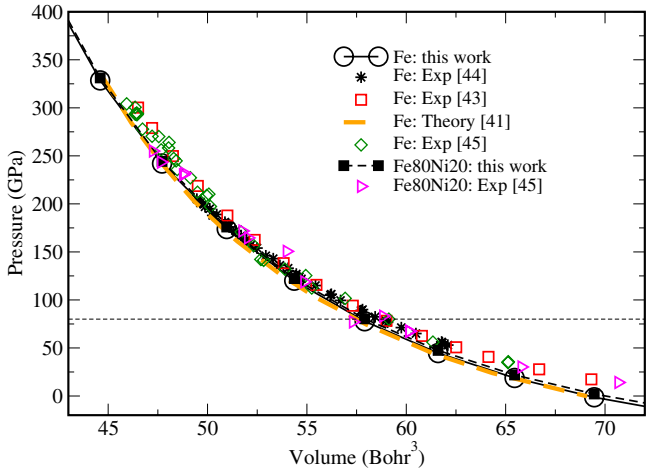

FIG. 3. (Color online) Pressure as function of volume in hcp $Fe_{80}Ni_{20}$ (dashed lines) and pure Fe (full lines). Experimental data for pure Fe by Dubrovinsky *et al.* (Ref. 43) are shown by (red) squares, Dewaele *et al.*44 by black stars while data for Fe and $Fe_{80}Ni_{20}$ by Mao *et al.* (Ref. 45) are shown by (green) diamonds and (magenta) triangles, respectively. For reference, calculations for pure Fe by Steinle-Neumann *et al.* (Ref. 41) are shown by a thick-dashed (orange) line. The thin and horizontal dashed line shows the limit below which hcp FeNi is likely to become magnetic.

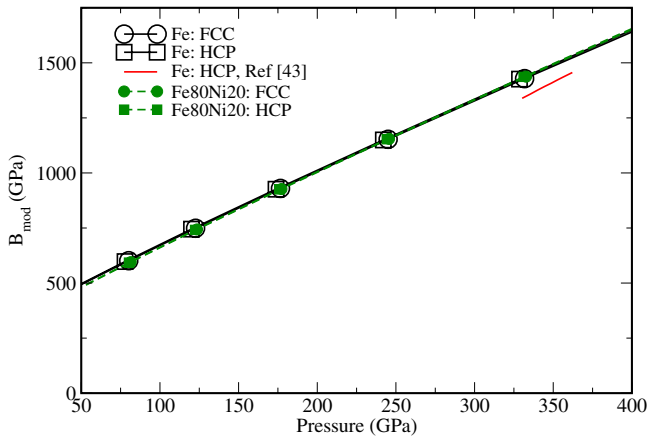

FIG. 4. (Color online) Bulk modulus as function of pressure in fcc (circles) and hcp (squares) $Fe_{80}Ni_{20}$ (green and dashed lines) and pure Fe (black and full lines). Shown by a (red) line are calculations for $T=5000$ K from experimental data by Dubrovinsky *et al.* (Ref. 43).

From the EOS we also calculated the density as function of Ni concentration, for the pressure 330 GPa. For both fcc and hcp phases, the density *increases* with increasing Ni concentration, though the dependence is rather weak. This behavior is also confirmed by experimental data from Mao *et al.*[45] In the fcc phase, the density changes from 14013 kg/m^3 for pure Fe to 14181 kg/m^3 for $Fe_{75}Ni_{25}$ while the corresponding numbers for hcp goes from 14 022 to 14 193 kg/m^3. Here it is worth to notice that for any Ni concentration in this work, the hcp density lies slightly above that of fcc.

In Fig. 4, the calculated bulk modulus as a function of pressure is shown together with experimental results of Dubrovinsky *et al.*[43] The data in Ref. 43 was obtained at high temperature and therefore our $T=0$ K calculations show slightly higher bulk modulus. Since Fe and Ni have similar bulk moduli and electronic structure and since we are in the nonmagnetic pressure range, changing the Ni concentration causes a very small change in bulk modulus. For both hcp and fcc phases, increasing the Ni concentration from 0 to 25 at % results in a decrease in the bulk modulus. In the high-pressure region, the change is very small (about 1%–2%) for both fcc and hcp phases. These features can be seen in Fig. 5 which shows the bulk modulus for fcc and hcp FeNi relative to that of pure Fe.

Next, Fig. 6 shows the calculated c/a ratio as a function of pressure in hcp FeNi, together with experimental results by Ma *et al.*[46] and Dewaele *et al.*[44] The agreement between our calculations and experiment is reasonable, though it should be pointed out that the two different sets of experimental data show opposite trends with increasing pressure. Experimental data by Mao *et al.*[45] is not shown in the figure since its spread is too large compared to the variation in c/a as function of pressure on the figure scale. In the pressure interval from 77 to 270 GPa, c/a for pure Fe varies between 1.620 and 1.575 in Ref. 45. Variations in c/a for the $Fe_{80}Ni_{20}$

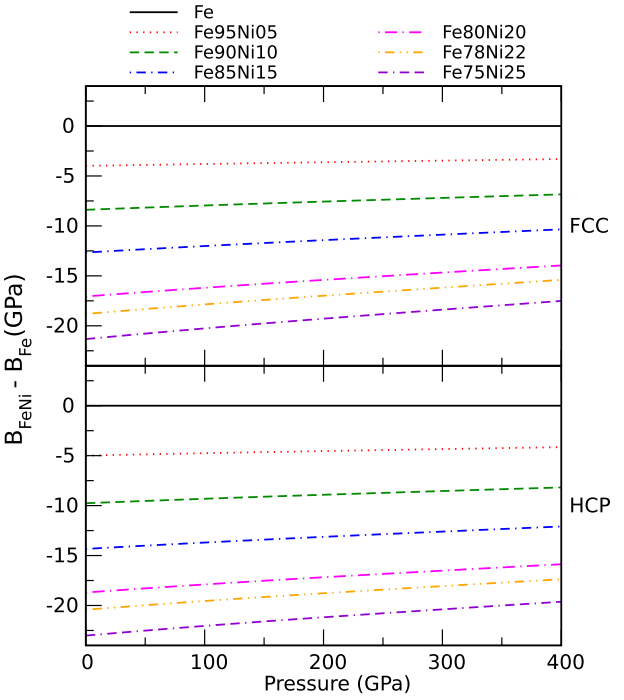

FIG. 5. (Color online) Bulk modulus (in GPa) as function of pressure in fcc (top) and hcp (bottom) FeNi relative to pure Fe.

alloy are between 1.674 and 1.552. The weak dependence of c/a ratio on pressure and the spread in experimental data-makes more general conclusions about the theoretical accuracy hard to draw. The calculated results are also in good agreement with the work of Sha *et al.*[47] and Gannarelli *et al.*[48] The c/a ratio increases with increasing Ni concentration and while this effect is small, it is still larger than the variation with pressure. We would like to point out that the minor differences in c/a ratio between this work and that in Ref. 13 is due to different interpolation methods. The effect of these differences upon the elastic constants and the anisotropy has been found to be negligible.

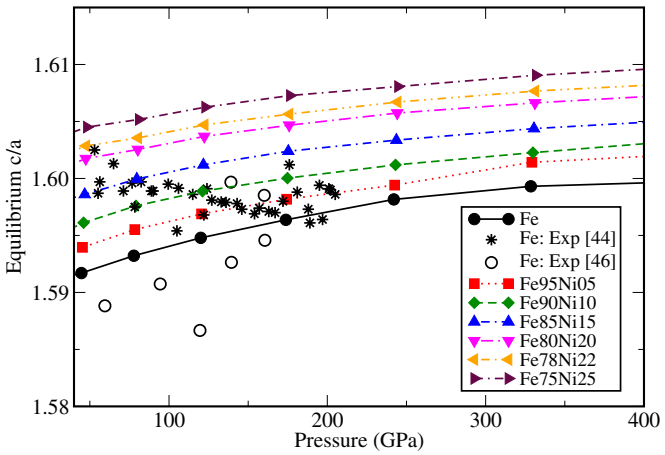

FIG. 6. (Color online) c/a ratio as function of pressure in hcp FeNi for different concentrations. Full symbols with lines to guide the eyes denote calculations while open circles and stars denote experimental results by Ma *et al.* (Ref. 46) and Dewaele *et al.* (Ref. 44), respectively. See text for more details.

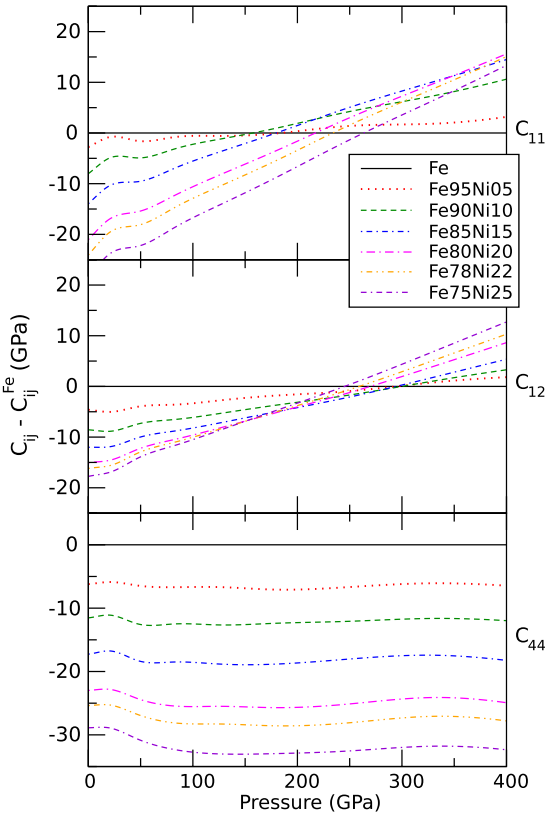

FIG. 7. (Color online) Single-crystal elastic constants as functions of pressure in fcc Fe (full lines) and $Fe_{80}Ni_{20}$ (dashed lines).

B. Single-crystal elastic constants

The single-crystal elastic constants of fcc Fe and $Fe_{90}Ni_{10}$ as functions of pressure are shown in Fig. 7. For fcc, the stability requirements for the elastic constants are[31]

$$c_{11} > |c_{12}|,$$

$$c_{12} + 2c_{12} > 0 \Leftrightarrow B > 0,$$

$$c_{44} > 0. \tag{21}$$

So, from Figs. 7 and 4 we conclude that the fcc phase of FeNi is elastically stable.

As expected, all elastic constants increase with increasing pressure. For c_{11} and c_{12} the effect of adding Ni in Fe is very small while it is slightly larger for c_{44}. The effect of adding Ni in Fe on c_{11} and c_{12} is very small, about 1 % when going from pure Fe to $Fe_{75}Ni_{25}$, which is of similar magnitude as the expected accuracy of the calculations of the elastic constants. At $V \approx 44.6$ Bohr^3 (about 330 GPa) c_{11} and c_{12} increase with increasing Ni content while the opposite situation is present for $V \approx 57.9$ Bohr^3 (about 80 GPa), though the shift is still of similar magnitude as the expected accuracy of the calculations and therefore it should be taken with care. When going from pure Fe to $Fe_{75}Ni_{25}$, the c_{44} elastic constant decreases about 3% at $V \approx 44.6$ Bohr^3 and about 6% at $V \approx 57.9$ Bohr^3. All these features can be found in Fig. 8. Unfortunately, there is a lack of experimental data for fcc FeNi at high pressure.

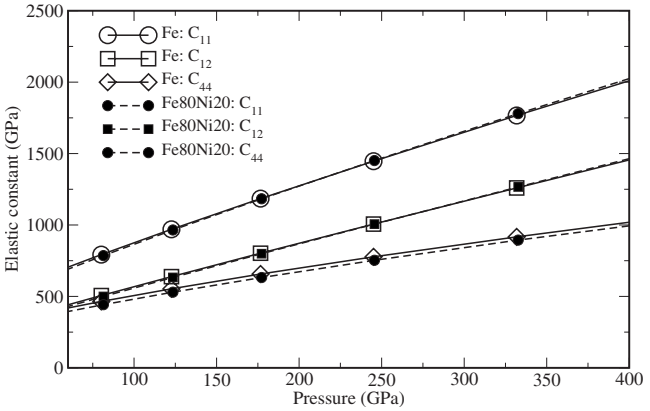

FIG. 8. Single-crystal elastic constants (in GPa) as functions of pressure in fcc FeNi, relative to pure Fe.

Turning to the hcp phase, the elastic constants of FeNi alloys are shown as function of pressure in Fig. 9. Also here all elastic constants increase with increasing pressure. The stability criterion for the *hcp* structure are the following:[31]

$$c_{11} > |c_{12}|,$$

$$c_{33}(c_{11} + c_{12}) > 2c_{13}^2 \Rightarrow B_R > 0,$$

$$c_{11}c_{33} > c_{13}^2,$$

$$c_{44} > 0. \tag{22}$$

All these requirements in Eq. (22) are fulfilled. A simple calculation verifies this remaining requirement of stability. So we may conclude that also hcp FeNi is elastically stable at all pressures, at least within the concentration range considered in this work.

Included in Fig. 9 are experimental data from Mao *et al.*,[49] Antonangeli *et al.*,[50] and Merkel *et al.*[51] Also shown are calculations at $T=0$ K by Steinle-Neumann *et al.*[12] It should be noted that we have put these calculations at a pressure corresponding to the volume used in Ref. 12. However, the pressure-volume relation in our work very closely match that of Steinle-Neumann *et al.* in Ref. 41. The overall agreement with experimental results is good, even though our calculations lie a bit above the experimental values for c_{11} and c_{12}. This could be because our calculations are done at 0 K but for c_{44} our results lie below that of Mao *et al.* Below about 80 GPa pressure, magnetism could still influence the results which may explain why c_{11} estimated by Antonangeli *et al.*[50] is softer than the 0 K calculations. The agreement between our calculations and those of Ref. 12 is excellent and this verifies the reliability of our method.

A summary of the behavior of the elastic constants when changing the Ni content from pure Fe to $Fe_{75}Ni_{25}$ is presented in Fig. 10, which shows the single-crystal elastic constants for hcp FeNi relative to Fe. In this figure we can see that when increasing the Ni concentration, the c_{11}, c_{12}, and c_{44} elastic constants decrease while the other two (c_{13} and c_{33}) show a rather small increase. It is also worth to notice that adding Ni has a larger effect on elastic constants in general for the hcp phase than for the fcc.

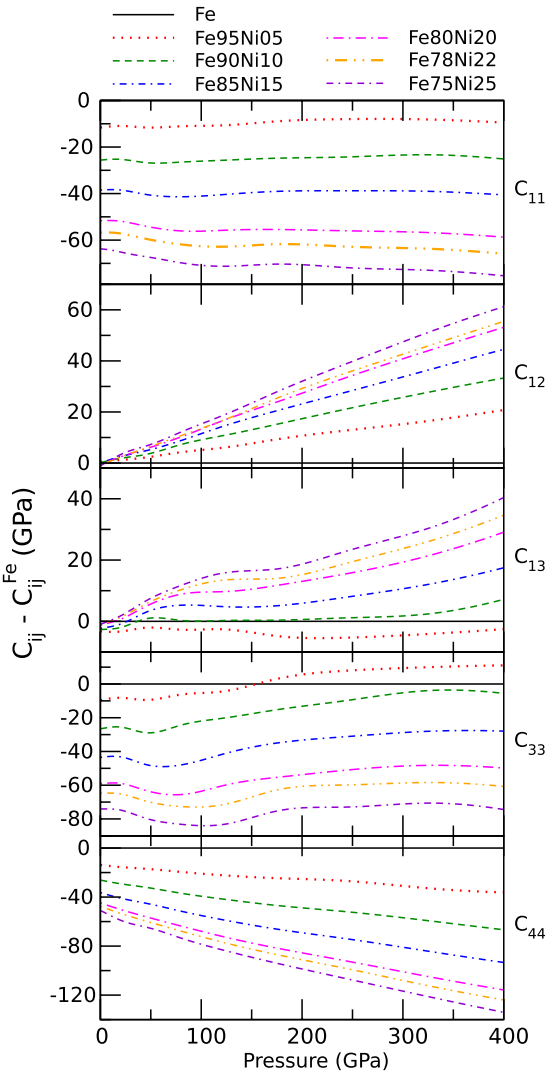

FIG. 9. (Color online) Single-crystal elastic constants as functions of pressure in hcp $Fe_{80}Ni_{20}$ (dashed lines) and pure Fe (full lines). Full symbols denote our calculations while open symbols denote experimental results: magenta from Mao *et al.* (Ref. 49) red from Antonangeli *et al.* (Ref. 50), and green from Merkel *et al.* (Ref. 51 Also shown many orange open symbols are calculations at $T=0$ K by Steinle-Neumann *et al.* (Ref. 12) See text for more details.

C. Polycrystalline elastic constants and anisotropy

Figure 11 shows the Voigt and Reuss shear moduli as functions of pressure in $Fe_{80}Ni_{20}$ and pure Fe. Here we note that for fcc the difference between Voigt and Reuss is much larger than for hcp. For fcc the difference between the moduli increases more with pressure, than it does for hcp. These findings can also be seen in Fig. 12 below. It is also worth noting that for hcp the both moduli change with increasing Ni content while for fcc the moduli change much less.

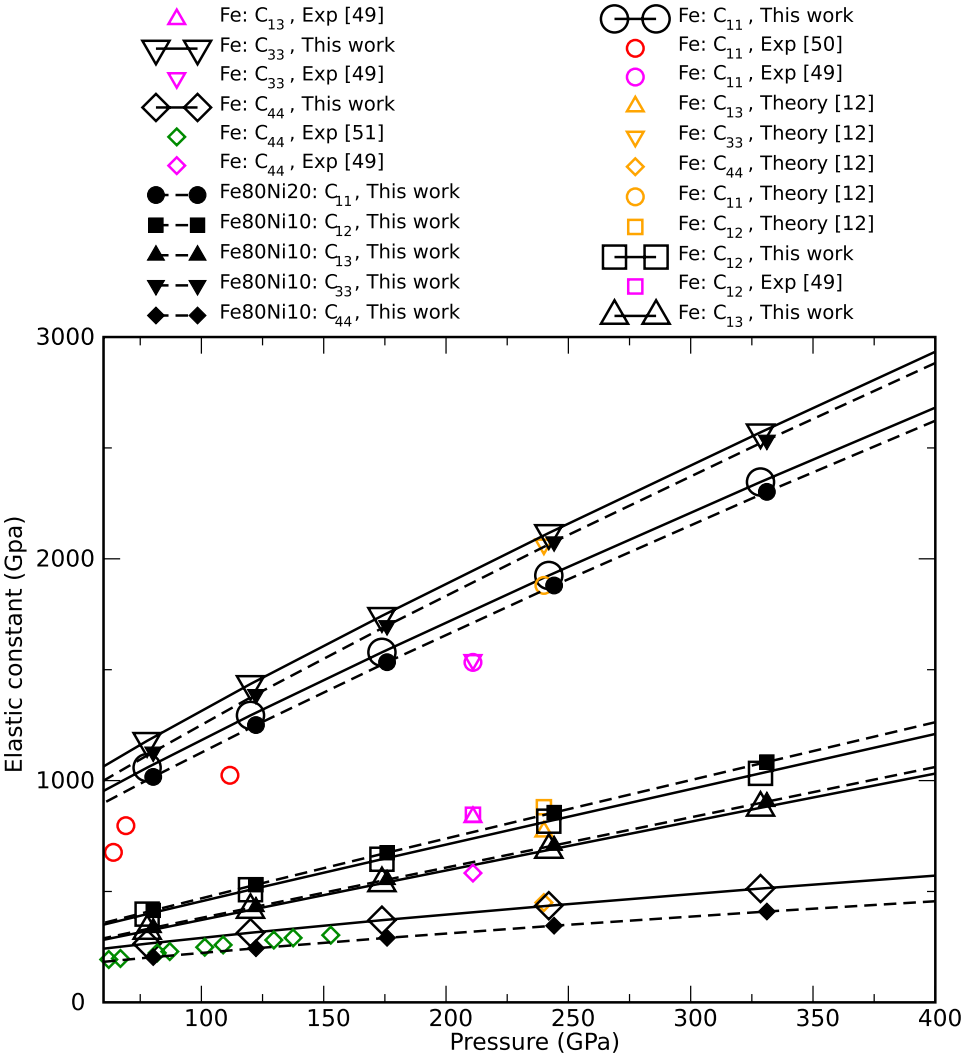

FIG. 10. (Color online) Single-crystal elastic constants (in GPa) as functions of pressure in hcp FeNi, relative to pure Fe.

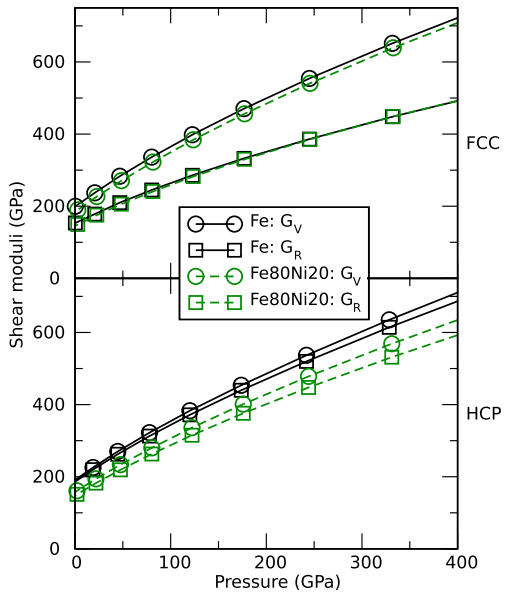

FIG. 11. (Color online) Voigt (circles) and Reuss (squares) shear moduli in pure Fe (full lines) and $Fe_{80}Ni_{20}$ (dashed lines) as functions of pressure. Top panel shows fcc and the bottom shows hcp.

The VRH anisotropy, defined in Eq. (20), is shown for fcc and hcp Fe and $Fe_{80}Ni_{20}$ alloy in Fig. 12. Also shown in this figure are the anisotropy for pure Fe extracted from calcula-

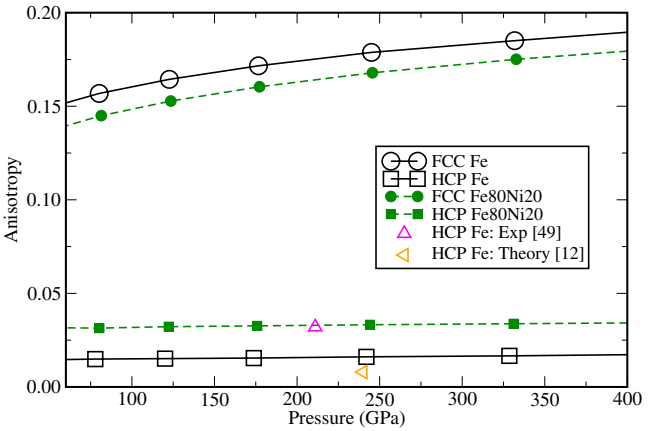

FIG. 12. (Color online) Elastic anisotropy in Fe and $Fe_{80}Ni_{20}$ as function of pressure. Experimental data for hcp Fe from Mao *et al.* (Ref. 49) are shown by magenta upward triangles while calculations for hcp by Steinle-Neumann *et al.* (Ref. 12) are shown by orange left triangles.

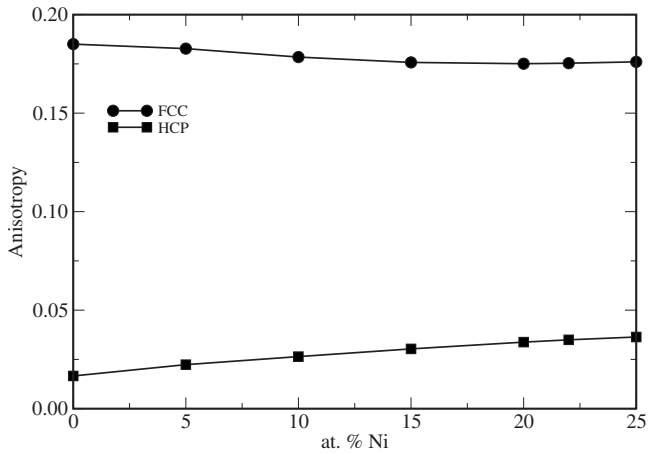

FIG. 13. Anisotropy for $V=44.6$ Bohr^3 (corresponding to $P \approx 330$ GPa) in FeNi as function of Ni concentration.

tions by Steinle-Neumann *et al.*[12] and experimental results from Mao *et al.*[49]

For the hcp anisotropy there is excellent agreement between our calculations and experiment. Our results also agree with those calculated by Steinle-Neumann *et al.*[12] The excellent agreement for the hcp anisotropy suggests that our calculations for the fcc phase are indeed reliable.

Several observations can be made from Fig. 12. First, and most interesting, the fcc systems are more anisotropic than hcp ones, which is unexpected since the fcc structure has a higher degree of symmetry. Moreover, the anisotropy of fcc FeNi increases with pressure and depends more strongly on pressure than the anisotropy for the hcp structure. The latter is almost constant in the pressure range studied in this work.

In Fig. 13 the calculated anisotropy for $V=44.6$ Bohr^3, corresponding to $P \approx 330$ GPa is shown as function of Ni concentration. Here it is interesting to notice that for the fcc structure the anisotropy decreases slightly with increasing Ni content while for hcp alloys the situation is the opposite. Since the hcp anisotropy is fairly close to zero, it is hard to measure the change in anisotropy with Ni content in percent. However, for $V=44.6$ Bohr^3 the hcp anisotropy is about 0.017 for pure Fe and increase to 0.036 for $Fe_{75}Ni_{25}$. This should be compared with the fcc anisotropy, which changes from about 0.185 for pure Fe to 0.176 for $Fe_{75}Ni_{25}$. Also, the dependence on Ni concentration is stronger for hcp than for fcc. However, adding Ni does not change the anisotropy ratio between fcc and hcp alloys qualitatively, that is, the elastic anisotropy is still much higher for the fcc crystals.

The numerical value of the VRH anisotropy is rather sensitive to changes in the elastic constants. In order to investigate the possible effects of temperature, especially together with the inclusion of disorder effects, more theoretical studies as well as experimental data is needed. Further studies should also include the bcc phase of FeNi. However, already at this stage we can make an important conclusion. Though the fcc results in this study differ from those extracted from Ref. 7, both agree qualitatively on that the VRH anisotropy is much higher for the fcc than for the hcp phase. Therefore we believe that our observation is of direct relevance for the studies of the elasticity of the earth's core, which currently attract substantial attention.

V. CONCLUSIONS

We have calculated the equation of state and elastic constants in fcc and hcp Fe-rich FeNi at high pressure and zero temperature from first principles. The disorder effects are fully taken into account within the coherent-potential approximation. For pure hcp Fe we find good agreement of our results with earlier calculations and with available experiment. It is found that adding Ni to Fe increases the density in both fcc and hcp phases. Also, adding Ni to Fe has a higher influence on the elastic constants of hcp alloys, as compared to fcc alloys. In particular, at highly compressed volumes, corresponding to the earth's core pressure, the c_{44} elastic constant of the hcp $Fe_{75}Ni_{25}$ alloy decreases by more than 20% in comparison with pure Fe. Although the decrease in c_{44} in the fcc phase is also found to be the largest among all other fcc elastic constants, it remains below 3%. Contrary to what is expected from intuition based on symmetry considerations, we find that the Voigt-Reuss-Hill elastic anisotropy is higher for the fcc phase than for the hcp. Though adding Ni decreases the elastic anisotropy in the fcc phase somewhat while it increases for the hcp phase, the former is much higher than the latter for any Ni concentrations considered in this study. We argue that the effect may also be present at high temperature.

ACKNOWLEDGMENTS

Discussions with L. Dubrovinsky and M. Ekholm are greatly acknowledged. We are grateful for financial support from the Swedish Research Council and the Göran Gustafsson Foundation for Research in Natural Sciences and Medicine. Computer support from the following supercomputer centers is acknowledged: NSC, UPPMAX, Swegrid, and HPC2N.

*chrgo@ifm.liu.se

[1] L. Dubrovinsky, N. Dubrovinskaia, O. Narygina, I. Kantor, A. Kuznetzov, V. B. Prakapenka, L. Vitos, B. Johansson, A. S. Mikhaylushkin, S. I. Simak, and I. A. Abrikosov, Science **316**, 1880 (2007).

[2] J.-F. Lin, D. L. Heinz, A. J. Campbell, J. M. Devine, and G. Shen, Science **295**, 313 (2002).

[3] L. Dubrovinsky, N. Dubrovinskaia, F. Langenhorst, D. Dobson, D. Rubie, C. Geszmann, I. A. Abrikosov, B. Johansson, V. I. Baykov, L. Vitos, T. Le Bihan, W. A. Crichton, V. Dmitriev, and H.-P. Weber, Nature (London) **422**, 58 (2003).

[4] A. B. Belonoshko, R. Ahuja, and B. Johansson, Nature (London) **424**, 1032 (2003).

[5] N. Dubrovinskaia, L. Dubrovinsky, I. Kantor, W. A. Crichton, V.

Dmitriev, V. Prakapenka, G. Shen, L. Vitos, R. Ahuja, B. Johansson, and I. A. Abrikosov, Phys. Rev. Lett. **95**, 245502 (2005).
[6] A. S. Mikhaylushkin, S. I. Simak, L. Dubrovinsky, N. Dubrovinskaia, B. Johansson, and I. A. Abrikosov, Phys. Rev. Lett. **99**, 165505 (2007).
[7] L. Vočadlo, I. G. Wood, D. Alfè, and G. D. Price, Earth Planet. Sci. Lett. **268**, 444 (2008).
[8] Y. Kuwayama, K. Hirose, N. Sata, and Y. Ohishi, Earth Planet. Sci. Lett. **273**, 379 (2008).
[9] L. Vočadlo, D. Alfè, M. J. Gillan, I. G. Wood, J. P. Brodholt, and G. D. Price, Nature (London) **424**, 536 (2003).
[10] L. Vočadlo, Earth Planet. Sci. Lett. **254**, 227 (2007).
[11] A. B. Belonoshko, N. V. Skorodumova, A. Rosengren, and B. Johansson, Science **319**, 797 (2008).
[12] Gerd Steinle-Neumann, Lars Stixrude, R. E. Cohen, and Oguz Gülseren, Nature (London) **413**(6851), 57 (2001).
[13] K. Kadas, L. Vitos, and R. Ahuja, Earth Planet. Sci. Lett. **271**, 221 (2008).
[14] L. Vitos, I. A. Abrikosov, and B. Johansson, Phys. Rev. Lett. **87**, 156401 (2001).
[15] D. Music, T. Takahashi, L. Vitos, C. Asker, I. A. Abrikosov, and J. Schneider, Appl. Phys. Lett. **91**, 191904 (2007).
[16] L. Vitos, *Computational Quantum Mechanics for Materials Engineers*, 1st ed. (Springer-Verlag, Berlin, 2007).
[17] V. Ozoliņš and M. Körling, Phys. Rev. B **48**, 18304 (1993).
[18] D. D. Johnson, F. J. Pinski, J. B. Staunton, B. L. Gyorffy, and G. M. Stocks, in *Physical Metallurgy of Controlled Expansion Invar-Type Alloys*, edited by K. C. Russell and D. F. Smith (TMS, Warrendale, PA, 1990), p. 3; D. D. Johnson and W. A. Shelton, in *The Invar effect: A Centennial Symposium*, edited by J. Wittenauer (TMS, Warrendale, PA, 1997), p. 63.
[19] H. Akai, J. Phys.: Condens. Matter **1**, 8045 (1989).
[20] H. Akai and P. H. Dederichs, Phys. Rev. B **47**, 8739 (1993).
[21] I. A. Abrikosov, O. Eriksson, P. Söderlind, H. L. Skriver, and B. Johansson, Phys. Rev. B **51**, 1058 (1995).
[22] M. Schröter, H. Ebert, H. Akai, P. Entel, E. Hoffmann, and G. G. Reddy, Phys. Rev. B **52**, 188 (1995).
[23] P. James, O. Eriksson, B. Johansson, and I. A. Abrikosov, Phys. Rev. B **59**, 419 (1999).
[24] V. Crisan, P. Entel, H. Ebert, H. Akai, D. D. Johnson, and J. B. Staunton, Phys. Rev. B **66**, 014416 (2002).
[25] A. V. Ruban, M. I. Katsnelson, W. Olovsson, S. I. Simak, and I. A. Abrikosov, Phys. Rev. B **71**, 054402 (2005).
[26] I. A. Abrikosov, A. E. Kissavos, F. Liot, B. Alling, S. I. Simak, O. Peil, and A. V. Ruban, Phys. Rev. B **76**, 014434 (2007).
[27] F. Birch, Phys. Rev. **71**, 809 (1947).
[28] G. Steinle-Neumann, L. Stixrude, and R. E. Cohen, Phys. Rev. B **60**, 791 (1999).
[29] P. M. Marcus and S. L. Qiu, J. Phys.: Condens. Matter **16**, 8787 (2004).
[30] Gerd Steinle-Neumann and R. E. Cohen, J. Phys.: Condens. Matter **16**, 8783 (2004).
[31] G. Grimvall, *Thermophysical Properties of Materials*, 1st ed. (Elsevier, New York, 1999).
[32] P. Hohenberg and W. Kohn, Phys. Rev. **136**, B864 (1964).
[33] W. Kohn and L. J. Sham, Phys. Rev. **140**, A1133 (1965).
[34] J. P. Perdew, K. Burke, and M. Ernzerhof, Phys. Rev. Lett. **77**, 3865 (1996).
[35] L. Vitos, J. Kollár, and H. L. Skriver, Phys. Rev. B **55**, 13521 (1997).
[36] O. K. Andersen, O. Jepsen, and G. Krier, *Exact Muffin-Tin Orbital Theory* (World Science, Singapore, 1994).
[37] L. Vitos, Comput. Mater. Sci. **18**, 24 (2000).
[38] L. Vitos, Phys. Rev. B **64**, 014107 (2001).
[39] P. Soven, Phys. Rev. **156**, 809 (1967).
[40] B. Velicky, S. Kirkpatrick, and H. Ehrenreich, Phys. Rev. **175**, 747 (1968).
[41] Gerd Steinle-Neumann, R. E. Cohen, and Lars Stixrude, J. Phys.: Condens. Matter **16**, S1109 (2004).
[42] V. L. Moruzzi, J. F. Janak, and K. Schwarz, Phys. Rev. B **37**, 790 (1988).
[43] L. S. Dubrovinsky, S. K. Saxena, F. Tutti, S. Rekhi, and T. LeBehan, Phys. Rev. Lett. **84**, 1720 (2000).
[44] A. Dewaele, P. Loubeyre, F. Occelli, M. Mezouar, P. I. Dorogokupets, and M. Torrent, Phys. Rev. Lett. **97**, 215504 (2006).
[45] H. K. Mao, Y. Wu, L. C. Chen, J. F. Shu, and A. P. Jephcoat, J. Geophys. Res. **95**, 21737 (1990).
[46] Y. Ma, M. Somayazulu, G. Shen, M. Ho-kwang, J. Shu, and R. J. Hemley, Phys. Earth Planet. Inter. **143-144**, 455 (2004).
[47] Xianwei Sha and R. E. Cohen, Phys. Rev. B **74**, 064103 (2006).
[48] C. M. S. Gannarelli, D. Alfè, and M. J. Gillan, Phys. Earth Planet. Inter. **152**, 67 (2005).
[49] H-K. Mao, J. Shu, G. Shen, R. J. Hemley, B. Li, and A. K. Singh, Nature (London) **396**, 741 (1998).
[50] D. Antonangeli, F. Occelli, H. Requardt, J. Badro, G. Fiquet, and M. Krisch, Earth Planet. Sci. Lett. **225**, 243 (2004).
[51] S. Merkel, A. F. Goncharov, M. Ho-kwang, P. Gillet, and R. J. Hemley, Science **288**, 1626 (2000).